DOI: 10.1002/ejic.201001260

pH-Sensitive Bis(2,2′:6′,2"-terpyridine)ruthenium(II) Complexes – A DFT/TDDFT Investigation of Their Spectroscopic Properties

Maria Grazia Lobello,[a] Simona Fantacci,[a,b] Alberto Credi,[c] and Filippo De Angelis*[a]

Keywords: Photophysics / Density functional calculations / Protonation / UV/Vis spectroscopy / Luminescence / Ruthenium

We report a DFT/TDDFT study on the geometric, electronic and optical properties of [Ru{4′-(4-pyridyl)-2,2′:6′,2"-terpyridine}$_2$]$^{2+}$. Because of the presence of the basic nitrogen atom on the terminal pyridyl ligands, in solution the complex can exist in three different protonation states depending on the pH, each with markedly different photophysical properties. We investigated the effect of protonation of the terminal pyridine groups on the electronic and optical properties of this Ru^{II} complex. TDDFT calculations in vacuo and aqueous solution were performed, finding good agreement between the simulated and the experimental absorption spectra, and reproducing the experimentally observed absorption redshift upon pyridine protonation. The calculated excited-state data provide a rationale for the luminescence properties observed by varying the solution pH, in terms of the different energy separation between MLCT and MC excited states in the complexes.

Introduction

Ru^{II}-polypyridyl complexes have attracted great interest for their unique photochemical and photophysical properties.[1–7] Among the various applications of such complexes are dye-sensitised solar cells, which are promising devices for the conversion of solar energy into electricity, whereby Ru^{II}-polypyridyl complexes have been identified as particularly efficient photosensitisers because of their broad range of visible light absorption, relatively long-lived excited states and high thermal stability.[8–12] The capability to transfer electrons and energy upon photoactivation coupled with the possibility to obtain different molecular architectures by ligand tuning, make Ru^{II}-polypyridyl complexes efficient photosensitizers in molecular machines and devices,[4,13] molecular wires for optoelectronics,[4,14] light harvesting dendritic antennas[4,13b,15,16] and systems for information processing.[13b,13c] Ru^{II}-polypyridyl complexes, because of their long wavelength absorption and the high quantum yield for the photogeneration of singlet oxygen, can also be utilized in photodynamic therapy.[17] Moreover, luminescent Ru^{II} complexes have been shown to behave as efficient sensors in physiological and environmental media,[18,19] DNA markers[20,21] and pH indicators.[22]

In this paper, we report a theoretical investigation of [Ru{4′-(4-pyridyl)-2,2′:6′,2"-terpyridine}$_2$]$^{2+}$, [Ru(tpy-py)$_2$]$^{2+}$,[22] and its protonated forms (Scheme 1). These complexes have demonstrated peculiar properties as molecular switches because of a luminescent signal in the red or far-red spectral region that can be switched on or off by the solution pH.[22]

The absorption spectra of these Ru complexes in the 220–800 nm spectral range exhibit bands typical of [Ru(tpy)$_2$]$^{2+}$-type compounds,[4] with intense bands in the near-UV region and a broad and moderately intense band in visible region.[22] The absorption spectra were measured at three different pH values of ca. 11, 4 and 2 in water, demonstrating that the absorption and luminescence spectra depend strongly on the solution pH. In particular, the visible band redshifts progressively with a decrease of the solution pH, the λ_{max} changing from 490 nm at basic pH to 497 nm at pH 4 and to 505 nm at acidic pH. The luminescence spectra exhibit a more complex and interesting behaviour;[22] the emission energy decreases on going from pH 11 to pH 4, and then slightly increases for more acidic solutions. Most notably, the measured emission lifetime significantly increases going from basic to acidic solutions. Hence, these Ru^{II} complexes can find potential applications as luminescent pH sensors and as molecular switches where a low-energy emission signal can be controlled chemically by an acid–base stimulation.

To provide a rationale for these experimental observations, with reference to the pH-dependent absorption and emission processes, and to gain insight into the relationship between the excited state energetics and the luminescence properties, we have investigated the photophysics of these complexes by means of DFT and time dependent DFT

[a] Istituto CNR di Scienze e Tecnologie Molecolari (ISTM-CNR), c/o Dipartimento di Chimica, Università di Perugia, Via elce di Sotto 8, 06213 Perugia, Italy
[b] Italian Institute of Technology (IIT), Center for Biomolecular Nanotechnologies, Via Barsanti, 73010, Arnesano, Lecce, Italy
[c] Dipartimento di Chimica "G. Ciamician", Università di Bologna, Via Selmi 2, 40126 Bologna, Italy
Supporting information for this article is available on the WWW under http://dx.doi.org/10.1002/ejic.201001260.

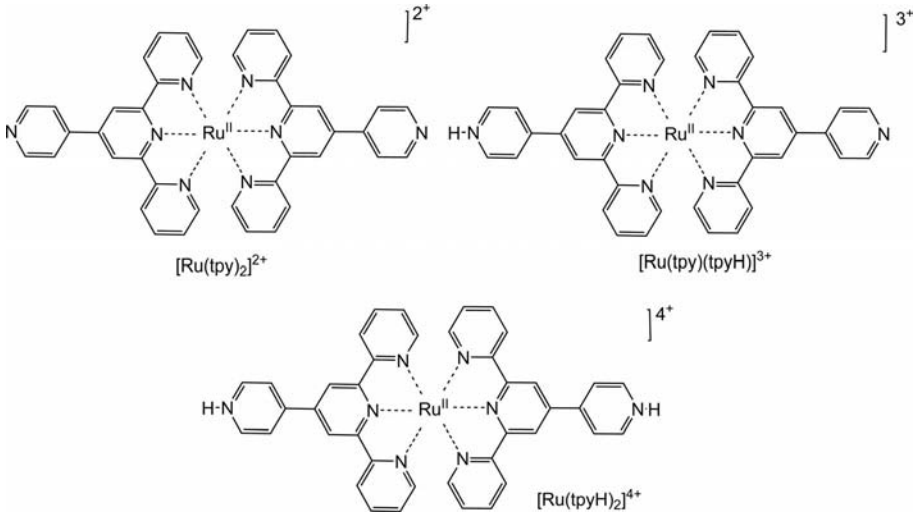

Scheme 1. Chemical structures of $[Ru(tpy\text{-}py)_2]^{2+}$ (Ru_0H), $[Ru(tpy\text{-}py)(tpy\text{-}pyH)]^{3+}$ (Ru_1H) and $[Ru(tpy\text{-}pyH)_2]^{4+}$ (Ru_2H).

(TDDFT) calculations. To investigate the effect of the solution pH on the optical properties, we have taken into account the protonation of one and both terminal pyridine units, simulating the absorption spectra and calculating the emission wavelengths of the protonated and nonprotonated forms.

Previous DFT/TDDFT calculations on Ru^{II} complexes have established the accuracy of this computational approach to describe the photophysics of this important class of compounds.[12,14,23–30]

Our computational approach satisfactorily reproduces the acidichromic shifts of the absorption spectra and allows us to interpret the pH-dependent emission lifetime variation in terms of the relative energetic positions of metal to ligand charge transfer (MLCT) and metal centred (MC) excited states in analogy to the classic photophysical picture of Balzani, Maestri and coworkers.[4] Theoretical data complement the previously reported experimental investigations, thus allowing a deeper understanding of the photophysics of these complexes, and opening the possibility for the design of new and more efficient functional complexes.

Computational Details

The absorption and luminescence spectra at three different pH values (ca. 11, 4 and 2) have been previously measured, see Ref.[22] for further details.

Following the experimental titration studies, we considered three different protonation states related to the different solutions pH values. In particular, the optical data measured at pH 11 were compared with the nonprotonated species $[Ru(tpy\text{-}py)_2]^{2+}$ (Ru_0H), whereas data related to solutions at pH 4 and 2 were compared with the monoprotonated $[Ru(tpy\text{-}py)(tpy\text{-}pyH)]^{3+}$ (Ru_1H) and biprotonated species $[Ru(tpy\text{-}pyH)_2]^{4+}$ (Ru_2H), respectively.

All the calculations were performed using the Gaussian03 (G03) program package.[31] Geometry optimizations of Ru_0H were performed in vacuo and aqueous solution, using the B3LYP[32] exchange-correlation functional. Two basis sets were tested: a LANL2DZ[33] for all atoms along with the corresponding pseudopotentials for Ru and a LANL2DZ basis set and pseudopotential for Ru augmented with a 6-31G*[34] basis sets for N, C and H atoms. Solvation effects were included by means of the polarizable continuum model (PCM),[35] as implemented in G03. We found the basis set and inclusion of solvation effects not to substantially influence the geometry of the Ru_0H complex, see below. For this reason, geometry optimizations of all the complexes were performed in vacuo with the LANL2DZ basis set for all atoms. The lowest SCF triplet state for all the species was optimized by unrestricted calculations at the same level of theory, to provide an estimate of the triplet excited state geometry. We then performed TDDFT calculations in aqueous solution on the structures optimized in vacuo. To take into account specific solute–solvent interactions on the geometrical electronic and optical properties, beyond the picture provided by continuum solvation models, we have optimized Ru_0H and Ru_1H including two and one water molecules bound to the pyridine nitrogen atoms. We define these systems as $Ru\_0H{\cdot}2H_2O$ and $Ru\_1H{\cdot}1H_2O$. Moreover, for Ru_0H we performed constrained geometry optimizations at selected values of the dihedral angle between the terpyridine and the pyridine planes to gauge the influence of this structural parameter on the optical properties.

Analysis of the electronic structures of all the complexes was carried out in aqueous solution. TDDFT calculations of the lowest singlet–singlet and singlet–triplet excitations were performed for all the species in aqueous solution at the same level of calculation employed for geometry optimizations, using the PCM nonequilibrium version[36] as implemented in G03. To simulate the optical spectra, the 70 lowest spin-allowed singlet–singlet transitions were computed on the ground state geometry. Transition energies and oscillator strengths were interpolated by a Gaussian convolution with a σ value of 0.15 eV. To investigate the emission

process, the lowest 30 singlet–triplet excitations were computed both on the singlet and triplet ground and excited state geometries.

Results and Discussion

Molecular and Electronic Structure

The geometry of Ru_0H was optimized considering a pseudo-octahedral C_2 symmetry (Figure 1). Moreover, to evaluate the effect of specific solute–solvent interactions, we optimized Ru_0H with two water molecules forming hydrogen bonds with the external pyridine nitrogen atoms (Ru_0H·2H_2O, Figure 1). In Table 1, the main optimized geometrical parameters are compared with experimental data.[37,38]

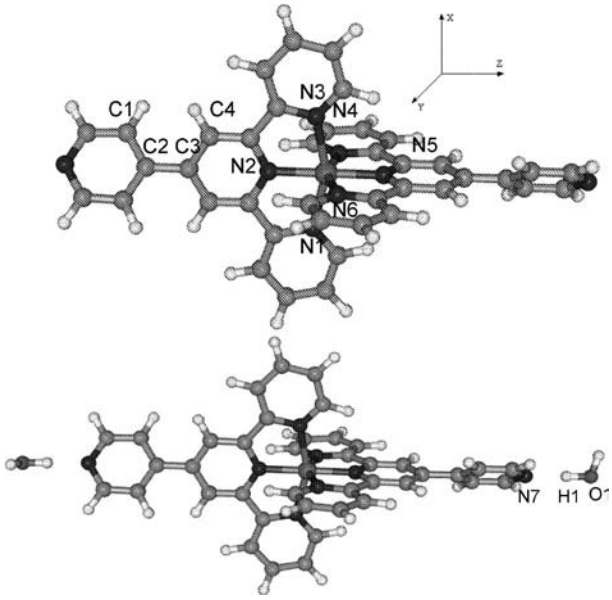

Figure 1. Optimized molecular structures of Ru_0H and Ru_0H·2H_2O.

Table 1. Main optimized geometrical parameters (Å and °) of Ru_0H in vacuo, in aqueous solution and with two water molecules (Ru_0H·2H_2O) compared with X-ray data from ref.[37]

Parameters	Experiment	Calculated		Calculated
		vacuum	water	water/2H_2O
Ru–N1	2.072(3)	2.111	2.106	2.107
Ru–N2	1.979(3)	2.010	2.003	2.003
N1–Ru–N2	78.34(13)	78.1	78.9	78.8
N2Ru–N4	102.50(13)	101.3	101.1	101.1

The agreement between the computed and experimental geometrical data is good, with the Ru–N2 bond of the central pyridines computed to be shorter than that of the peripheral rings, consistent with the X-ray data. Although a slight overestimation of main bond lengths compared to experimental data is observed, the optimized geometry reflects the main structural features of the compounds. As seen from Table 1, geometry optimization in solution leads to only modest geometrical variations. It is worth noting that the inclusion of two explicit water molecules close to the pyridine nitrogen atoms delivers only small geometrical differences in line with the geometry optimization in aqueous solution.

The main geometrical parameters of all the complexes, optimized both at the ground and lowest triplet states, are collected in Table 2. For Ru_1H, we optimized the ground state geometry in aqueous solution and included one water molecule interacting with the nonprotonated pyridine nitrogen atom. The optimized parameters (see Supporting Information) are marginally affected by the inclusion of implicit or explicit solvation effects, therefore geometries in vacuo will be considered for the remainder of our investigation.

Table 2. Optimized geometrical parameters (Å and °) of Ru_0H/1H/2H complexes in vacuo. Data of the lowest triplet state are reported in parentheses.

Parameters	Ru_0H	Ru_1H		Ru_2H
		Tpy-py	Tpy-pyH	
M–N1	2.110	2.116	2.109	2.116
	(2.097)	(2.106)	(2.100)	(2.106)
M–N2	2.010	2.022	1.995	2.011
	(2.013)	(2.024)	(2.011)	(2.019)
C2–C3	1.486	1.484	1.487	1.493
	(1.485)	(1.483)	(1.457)	(1.479)
N1–M–N2	78.1	78.3	79.0	78.6
	(79.2)	(79.1)	(79.0)	(79.0)
N1–M–N5	101.3	101.0	102.0	101.4
	(100.7)	(101.0)	(101.0)	(101.0)
∠C1C2C3C4	33.7	35.2	38.0	34.5
	(32.5)	(32.3)	(10.0)	(24.8)

Comparing the ground state optimized geometries of Ru_2H with those of Ru_0H we found minimal differences, indicating that the symmetric protonation of both terminal pyridines has a negligible effect on the ground state geometry.

The geometries of the lowest triplet state were found to be similar to the corresponding singlet ground state geometries for factors concerning the metal–ligand interactions, whereas sizeable differences have been computed for the ∠C1C2C3C4 dihedral angles, which measure the planarity of the terminal pyridines rings compared to the terpyridine core. In particular, for Ru_1H the ∠C1C2C3C4 dihedral angle of the lowest triplet state decreases drastically for the protonated pyridine ligand, whereas the same value as in the ground state is calculated for the nonprotonated ligand. Thus, protonation induces an asymmetry in the charge distribution of the excited states of the monoprotonated complexes. In the Ru_2H complex, a reduction of the dihedral angle is still computed but the difference between ground state and excited state is less pronounced than in Ru_1H and symmetrically distributed between the two ligands.

A schematic representation of the energy levels and the isodensity plots of selected frontier molecular orbitals of Ru_xH complexes are shown in Figure 2. The set of quasi-degenerate HOMO, HOMO-1 and HOMO-2 of all the investigated complexes have essentially Ru t_{2g} character while the LUMOs of the complexes are terpyridine π* orbitals, with different electronic localization depending on the pro-

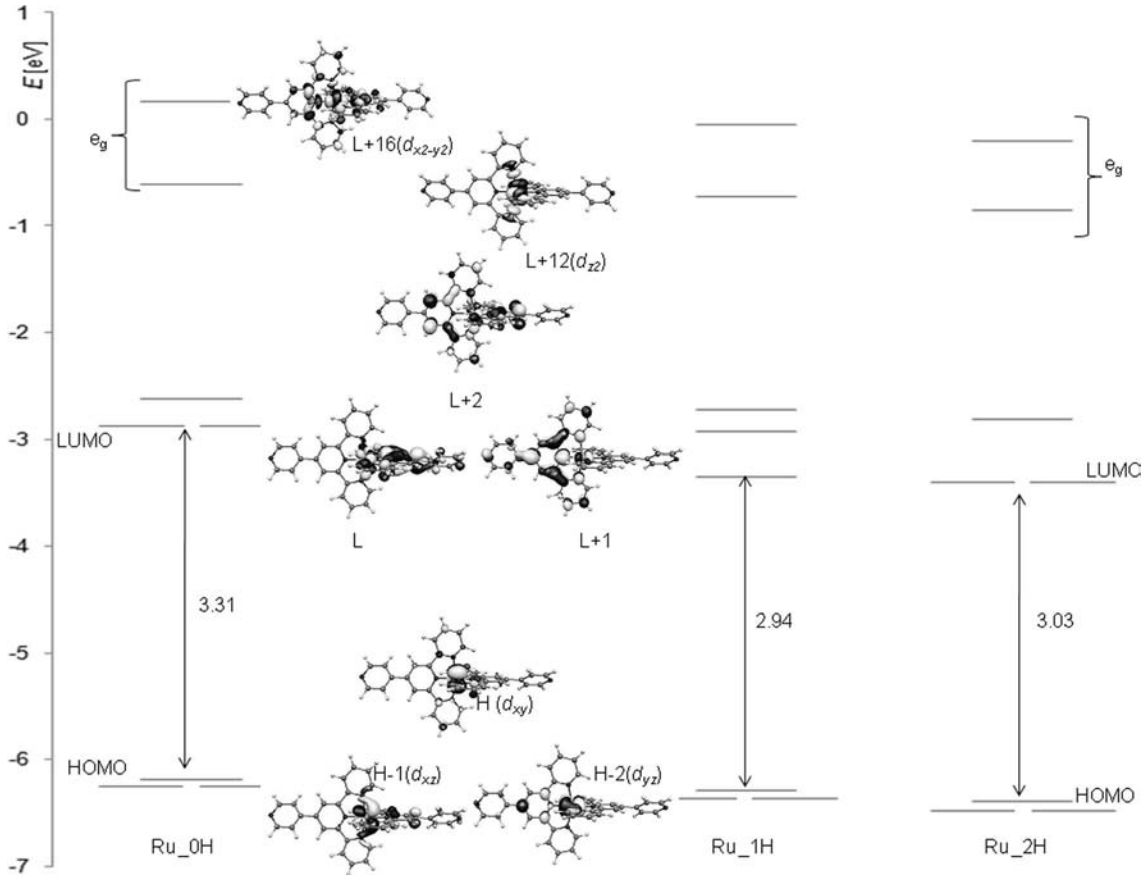

Figure 2. Schematic representation of the energy levels of the Ru_0H/1H/2H complexes. Isodensity surface plots (isodensity contour: 0.035) of selected Ru_0H molecular orbitals are also shown.

tonation. In Ru_0H and Ru_2H, the LUMO and LUMO+1 are degenerate and localized on both terminal pyridine units, whereas in Ru_1H the orbital degeneracy is lifted, with the LUMO mainly localized on the protonated pyridine and stabilized by 0.42 eV with respect to the LUMO+1, which maintains the same energy as that of the Ru_0H complex. For all the complexes, the LUMO+2 is localized on the tpy core, hence it is not influenced by protonation. The relevant e_g states are found for Ru_0H, Ru_1H and Ru_2H as the LUMO+12/+16, LUMO+13/+16 and LUMO+14/+15, respectively, see Figure 2.

For sake of completeness, we also analyzed the electronic structure of Ru_0H·2H_2O and Ru_1H·1H_2O (Supporting Information), finding minimal differences on the energy and character of the frontier molecular orbitals with respect to the nonexplicitly solvated systems.

Absorption Spectra

We simulated the absorption spectra of the complexes in the 250–600 nm spectral range considering the three different protonation states. A comparison between the experimental absorption spectrum measured at pH 11.5[22] and the spectra of the corresponding nonprotonated Ru_0H and Ru_0H·2H_2O species computed in aqueous solution is shown in Figure 3, and in Table 3 we report a comparison between the experimental and calculated absorption maxima for Ru_0H/1H/2H. Inset in Figure 3 is shown the comparison between the absorption spectra computed in vacuo and solution for Ru_0H. A blueshift of the main absorption

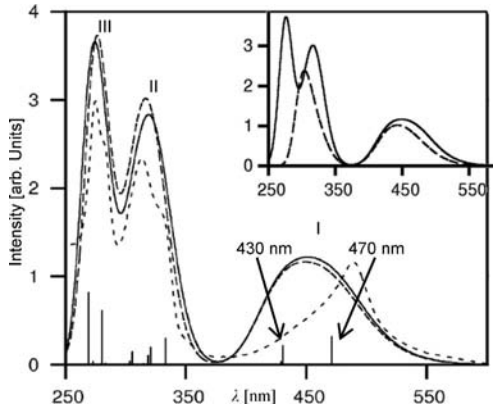

Figure 3. Comparison between calculated spectra of the Ru_0H (solid line) and Ru_0H·2H_2O (long dashed line) and the experimental spectrum at solution pH 11.5 (dashed line). Vertical lines correspond to calculated excitation energies and oscillator strengths for Ru_0H. Inset: comparison between the absorption spectra computed in vacuo (dashed line) and solution (solid line).

features is computed in vacuo with respect to that calculated in water. The absorption spectra of the complexes are typical of the class of Ru-polypyridyl compounds, with low energy MLCT transitions followed at higher energy by more intense $\pi \rightarrow \pi^*$ excitations.[4]

Table 3. Comparison between experimental and calculated (in parentheses) main UV/Vis absorption features [nm] of Ru_0H/1H/2H.

	III	II	I
Ru_0H	275 (276)	313 (317)	490 (470)
Ru_1H	275 (279)	313 (315)	497 (494)
Ru_2H	275 (275)	340 (349)	505 (499)

In the experimental UV/Vis spectrum at pH 11.5 we identified three main bands at 490, 313 and 275 nm, labelled I, II and III, respectively. The agreement between the computed Ru_0H spectrum in aqueous solution with the experimental spectrum at pH 11.5 is satisfactory, even though the visible absorption band is blue-shifted compared to the experiment (450 vs. 490 nm). The visible absorption band originates from the overlap of two transitions, computed at 430 and 470 nm. The discrepancy between the experimental and calculated spectra seems to be due to the overestimated intensity of computed transition at 430 nm, which is comparable to the intensity of the transition at 470 nm. The computed transition at 470 nm, is blue-shifted by 0.16 eV compared to the experimental band maximum at 490 nm, whereas the slightly less intense transition computed at 430 nm, is related to the small experimental shoulder measured at ca. 450 nm.

The simulated absorption spectrum of Ru_0H·$2H_2O$ is almost equivalent to that of Ru_0H, in terms of position of the bands, relative intensity and character (see Figure 3), therefore demonstrating that the discrepancy retrieved between the simulated and measured visible spectra cannot be attributed to specific solute–solvent interactions.

The presence of a single C–C bond between the terpyridine and pyridyl units opens the way to an internal rotation of the pyridyl ring around this bond, which might have an impact on the optical properties of Ru_0H. The ∠C1C2C3C4 dihedral angle measures the torsion of the pyridine with respect to the terpyridine plane; in the optimized Ru_0H structure in vacuo (water), this dihedral angle is 33.7° (31.8°). Since the transition at 470 nm involves the terminal pyridines, see below, we evaluated the effect of variation of the ∠C1C2C3C4 dihedral angle on the optical properties and optimized the molecular structures of Ru_0H fixing the ∠C1C2C3C4 dihedral angle at 20.0°, 10.0° and 0.0° computing the lowest 15 transitions on the optimized conformers. The computed energy difference in solution (ΔE shown inset in Figure 4) between the optimized Ru_0H and the structures with fixed dihedral angles of 20.0, 10 and 0° amounts to 0.15, 0.82 and 1.23 kcal/mol, respectively, and slightly higher energy differences are computed in vacuo. These results highlight the flexibility of the torsional mode considered, therefore making conformers with smaller ∠C1C2C3C4 dihedral angles accessible at room temperature.

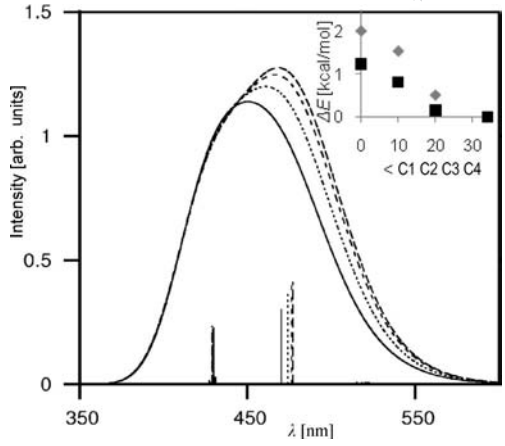

Figure 4. Simulated lowest absorption band of Ru_0H as a function of the ∠C1C2C3C4 dihedral angle. The curve and lines in solid, dotted, dashed and long dashed represent ∠C1C2C3C4 = 33.8°, 20.0°, 10.0° and 0.0°, respectively. Inset: plot of the relative energy (ΔE in kcal/mol) vs. the ∠C1C2C3C4 dihedral angle (dihedral). The ΔE values are the energies of the optimized molecular structures at different fixed ∠C1C2C3C4 dihedral angles, using the energy of the Ru_0H freely optimized structure characterized by a dihedral angle of 33.7° as a reference. Black squares refer to ΔE computed in vacuo, and grey diamonds refer to data in water.

The calculated absorption spectra in the visible region as a function of the ∠C1C2C3C4 dihedral angle are reported in Figure 4. It can be noted that by reducing the ∠C1C2C3C4 dihedral angle a sizeable redshift of the absorption maximum is found, with an associated increased band asymmetry. This is due to two concomitant effects, i.e. the slight redshift of the lowest transition from 470 to 477 nm, and its increased oscillator strength with respect to the transition at ca. 430 nm whose oscillator strength remains constant, see also Supporting Information. A better agreement with the experimental spectrum at pH 11.5 is obtained for the planar arrangements of Ru_0H so we speculate that the dynamics of the torsional mode, accessible at room temperature, might be responsible for the spectral asymmetry observed experimentally.

In Figures 5 and 6 we report the comparison between the experimental UV/Vis spectra measured at solution pH 4.1 and 2 and those computed for the mono- and diprotonated forms, respectively.

The calculated spectrum of Ru_1H is in good agreement with the experiment. Analogous to the spectrum of Ru_0H, we computed a substructured band originating from two transitions, one more intense at 494 nm, blue-shifted by only 0.01 eV with respect to the experimental maximum in the visible region, and one at 428 nm, which is directly related to the experimental feature found at 450 nm. Also in this case, the inclusion of the water molecule does not imply significant changes in the absorption spectrum of Ru_1H, see Figure 5. It is interesting to note that the simulated Ru_0H and Ru_1H spectra reproduce the experimental redshift of the visible absorption band on decreasing the solution pH.

The computed spectrum of Ru_2H in water is also in good agreement with the experimental data, Figure 6. In

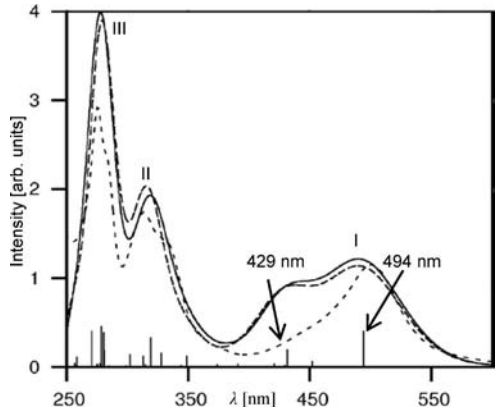

Figure 5. Comparison between the calculated spectra of Ru_1H (solid line) and Ru_1H·1H_2O (long dashed line) and the experimental spectrum at solution pH 4 (dashed line). Vertical lines correspond to calculated excitation energies and oscillator strengths of Ru_1H.

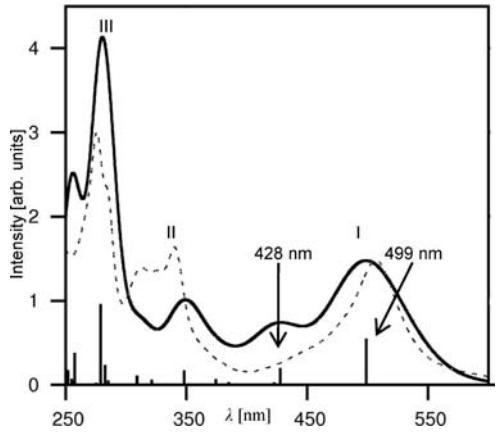

Figure 6. Comparison between the simulated spectrum of Ru_2H (solid line) and the experimental spectrum at pH 2 (dashed line). Vertical bars correspond to calculated excitation energies and oscillator strengths.

the visible region the lowest transition is further red-shifted with respect to that simulated for Ru_1H, as found experimentally, whereas the transition at 428 nm, which provides the characteristic band shape of the experimental spectrum, is computed at similar energies for the nonprotonated and protonated forms.

In summary, we are able to reproduce the changes in the UV region of the experimental absorption spectra at different solution pH values. In particular, on going from basic to acid pH the intensity of experimental absorptions maxima at 313 nm decreases. Moreover, going from pH 11.5 to pH 2 the shoulder at ca. 330 nm is red-shifted, substantially increasing in intensity. Band III is found at the same wavelength (275 nm) for all pH values.

The computed Ru_0H spectrum shows two bands of comparable intensity at 317 and 276 nm, see Figure 3, whereas in the Ru_1H spectrum the bands are computed at 315 and 279, the former being less intense than that of the neutral Ru_0H species, see Figure 5. The computed Ru_2H spectrum shows the appearance of a band at 349 nm, and an intensity decrease of the feature at ca. 315 nm, consistent with the experiment, see Figure 6. Hence, we can accurately simulate the experimental data also in the UV region, and the computed spectra reproduce the measured redshift. Moreover, we are also able to qualitatively estimate the relative intensity between bands II and III.

For the three Ru complexes, we assign the two computed low-energy transitions, constituting band I, as MLCT transitions, originating from the Ru t_{2g} orbitals, and arriving at the LUMO, LUMO+1 and LUMO+2 orbitals, localized on the tpy-py ligands, see Table 4. In particular, the lowest transition is dependent on the protonation state, and is essentially composed of HOMO-1→LUMO and HOMO-2→LUMO+1 transitions. Recalling the electronic structure discussed in Figure 2, the LUMO and LUMO+1, mainly localized on the terminal pyridine groups, are strongly affected by the nitrogen protonation, resulting in the redshift of the computed lowest absorption band. We also found that the main singlet–singlet transitions of Ru_0H·2H_2O are similar in character to those of Ru_0H, see Table 4 and Supporting Information. The lowest Ru_0H and Ru_2H transitions show a similar composition in terms of molecular orbitals, see Table 4. On the other hand, for Ru_1H we computed a sizeable contribution (69%) from HOMO-2→LUMO excitation. In this case, monoprotonation introduces an asymmetry in the electronic distribution, stabilizing the LUMO and localizing it on the protonated pyridine unit. The transition at ca. 430 nm, has essentially HOMO→LUMO+2 nature for all of the complexes, with the LUMO+2 localized on the tpy core ligand. This ex-

Table 4. Computed excitation energies (eV and nm) and oscillator strengths (*f*) for the optical transitions of the first absorption band of Ru_0H, Ru_0H·2H_2O, Ru_1H, Ru_1H·1H_2O and Ru_2H in aqueous solution.

	State	*E* [eV]	*WL* [nm]	*f*	Composition	
Ru_0H	5	2.64	470	0.303	H-2→L+1	43%
					H-1→L	43%
					H→L+2	8%
	9	2.88	430	0.230	H-2→L+1	3%
					H-1→L	3%
					H→L+2	89%
Ru_0H·2H_2O	5	2.63	471	0.327	H-2→L+1	43%
					H-1→L	43%
	7	2.88	431	0.225	H→L+2	84%
Ru_1H	4	2.51	494	0.387	H-2→L	69%
					H-1→L +1	12%
					H→L+2	7%
					H→L+3	2%
	9	2.90	429	0.193	H-2→L	4%
					H→L+2	81%
					H→L+3	11%
Ru_1H·1H_2O	4	2.50	494	0.410	H-2→L	69%
					H-1→L+1	13%
	7	2.87	431	0.200	H→L+2	79%
					H→L+3	10%
Ru_2H	5	2.49	499	0.549	H-2→L+1	44%
					H-1→L	44%
					H→L+2	3%
	7	2.90	428	0.199	H→L+2	94%

plains why this feature is not influenced by protonation, lying at essentially the same energy for the three protonation states.

The inclusion of one water molecule does not affect the character of the transitions giving rise to the Ru_1H simulated absorption spectrum, see Table 4.

Among the computed π–π* transitions we identified two main pH-dependent transitions. For Ru_0H these two transitions are degenerate and characterized by the same oscillator strength, and involve, as the arrival orbitals, the degenerate LUMO couple localized on each outer pyridine nitrogen centre. For Ru_1H, one of these transitions remains at 322 nm, whereas that involving the LUMO on the protonated pyridine is strongly red-shifted (348 nm). For Ru_2H the two transitions are characterized by the same energy and character (348 nm). For each complex we also found MC transitions, in which an electron is promoted from a Ru-based molecular orbital belonging to the filled metal t_{2g} shell to the empty metal e_g orbitals. We identified two such MC transitions for all complexes at ca. 360 and ca. 278 nm, both with negligible oscillator strengths.

Luminescence Spectra

A survey of the experimental photophysical emission data for the Ru complexes at various pH values is reported in Table 5, and the emission profile as a function of pH solution are reported in Figure 7.

Table 5. Experimental emission energy (em. energy), quantum yield (Φ_{em}), lifetime (τ) and nonradiative constant (k_{nr}) for Ru_0H/1H/2H in aqueous solution measured at pH 11.5, 4.1 and 2.

pH	Em. energy [eV]	$\Phi_{em} \times 10^2$	τ [ns]	k_{nr}
11.5	1.90	0.012	8	0.1235
4.1	1.75	0.027	88	0.0111
2	1.78	0.043	118	0.0081

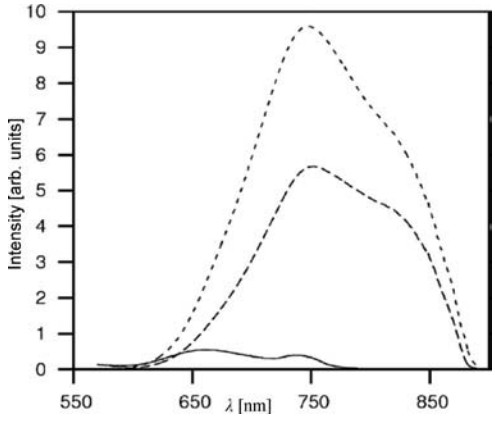

Figure 7. Experimental luminescence spectra at solution pH 11.5 (solid line), pH 4.1 (dashed line) and pH 2 (dotted line).

The energy of the emission maximum decreases going from pH 11 to pH 4 and then slightly increases for more acidic solutions. On decreasing the solution pH, a marked increase in the emission lifetimes and quantum yields was found,[22] from which a substantial decrease in the nonradiative deactivation rate constant (k_{nr} in Table 5) can be calculated. The k_{nr} decrease observed going from basic to acidic pH is in contrast with the energy gap law,[39] which predicts an increase of the rate of nonradiative deactivation processes by decreasing the emission energy.

To provide a rationale for these experimental findings, we calculated the lowest 30 singlet–singlet and singlet–triplet excitations at the singlet and the triplet optimized geometries. In particular, we related the emission energies measured in solution at pH 11 with the lowest TDDFT singlet–triplet energy computed for the nonprotonated species and the phosphorescence measured at ca. pH 4 and 2 with the lowest singlet–triplet transition computed for the mono- and diprotonated forms, respectively.

In Table 6 we report the lowest singlet–singlet and singlet–triplet excitation energies for Ru_0H/1H/2H calculated at their singlet and triplet optimized geometries.

Table 6. Experimental and calculated emission energies (eV) for Ru_0H/1H/2H in aqueous solution.

Energy	Ru_0H		Ru_1H		Ru_2H	
	OPT_S	OPT_T	OPT_S	OPT_T	OPT_S	OPT_T
$S_0 \rightarrow T_1$	2.31	2.26	2.13	1.86	2.18	1.95
$S_0 \rightarrow S_1$	2.41	2.30	2.17	1.88	2.22	2.07

A precise comparison between experimental emission maxima and theoretical data would require simulation of the emission profiles for the various species;[40] however, here we limit our attention to the nonvibronically resolved transition energies. By looking at the data in Table 6, we notice that for both singlet and triplet geometries, the calculated data reproduce the redshift of the emission maxima observed experimentally.

In particular, the differences among the singlet–triplet transition energies for Ru_0H, Ru_1H and Ru_2H computed at the singlet geometry are very similar to those experimentally observed, whereas the differences associated to the computed singlet–triplet excitation energies at the triplet geometry are found to be larger with respect to the experimental findings. This behaviour might be associated to some extent with inaccuracies in the geometries of the triplet excited states calculated here by simple unrestricted calculations. It seems therefore reasonable, for the purpose of a qualitative analysis, to consider the singlet geometry as an estimate of the emission energies of the different species, and hereafter we refer to transitions at singlet geometry.

The lowest singlet–triplet transition has a MLCT character for all the Ru species. The redshift of the luminescence band on going from Ru_0H to Ru_1H is due to a stabilization of the MLCT level, which involves as the final state the tpy-pyH π* orbital, which is markedly affected by protonation. The slight blueshift of the luminescence band on going from Ru_1H to Ru_2H is related to a slight destabilization of Ru_2H MLCT levels, see Figure 8.

It can be noted from Figure 8 that the energy gap between the MLCT and MC excited states is found to increase

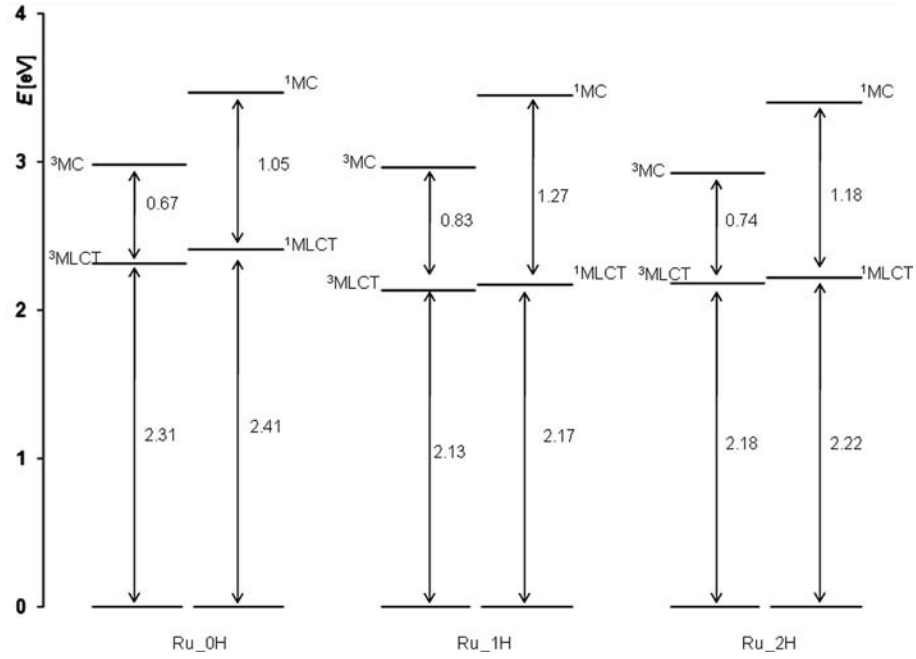

Figure 8. Schematic representation of the ^{1}MLCT, ^{1}MC and ^{3}MLCT, ^{3}MC energy levels of Ru_0H and its protonated forms calculated at the ground state geometry.

on going from Ru_0H to Ru_1H and then to slightly decrease for Ru_2H, in line with the experimental k_{nr} trend, showing a nonradiative constant decrease on going from Ru_0H to Ru_2H. This behaviour is related to the relationship between the MLCT and MC energy gap and the nonradiative constant. Indeed, as the energy gap between the MLCT and MC states decreases, the probability for the MC levels to be populated from the lowest MLCT states increases.[1] Considering the dissociative nature of MC transitions associated with antibonding metal–ligand interactions, population of such states from the lower-lying MLCT states increases the probability that the excited state deactivates through nonradiative processes by means of large-amplitude molecular distortions, leading to reduced lifetimes and quantum yields and ultimately to larger nonradiative deactivation constants.

Conclusions

We have reported a theoretical investigation on the photophysical properties of terpyridine-based Ru^{II} complexes bearing a pyridine unit in the 4′-position of each tpy ligand. Because of the presence of such pyridine units, these compounds can exist in three different protonated forms. The electronic, structural and optical properties of all the possible complexes have been investigated by means of combined DFT/TDDFT calculations. The geometries of the complex and its protonated forms have been optimized in both the ground and lowest triplet excited states.

The absorption spectra simulated in aqueous solution reproduce the trend of the experimental data well. Our results quantitatively reproduce the redshift exhibited by the $[Ru(tpy\text{-}py)_2]^{2+}$ compounds on protonation. We assign the band in the visible region to MLCT transitions originating from Ru t_{2g} orbitals to π* orbitals of the tpy-py ligands. The localization of the lowest-lying excited states strongly depends on protonation of the terminal pyridine ligands, with the excited states of the protonated complexes being localized on the protonated pyridine ligands.

Furthermore, we have calculated the emission energies as a function of protonation, obtaining the experimental luminescence redshift observed experimentally. Our theoretical approach allows us to explain the experimental trend of quantum yields and nonradiative deactivation rate constants in terms of the relative energetic positions of MLCT and MC excited states, with population of lower-lying MC states held responsible for the reduced quantum yields and emission lifetimes observed for the nonprotonated Ru^{II} compound. Our theoretical analysis allows us to unravel the detailed atomistic features constituting the basis for the switching behaviour of these compounds, and opens the possibility for the design of new and more efficient functional complexes.

Supporting Information (see footnote on the first page of this article): Optimized geometrical parameters of Ru_1H in vacuo and aqueous solution and of Ru_1H·1H_2O. Energies of the frontier molecular orbitals of Ru_0H and Ru_0H·2H_2O, Ru_1H and Ru_1H·1H_2O, and Ru_2H. Excitation energies, oscillator strengths and composition of the optical transitions of the lowest absorption band of the Ru_0H complexes taking fixed the ∠C1C2C3C4 dihedral angle at 33.7°, 20.0°, 10.0° and 0.0° in aqueous solution.

EurJIC European Journal of Inorganic Chemistry

Acknowledgments

We thank Professor Ed Constable and his coworkers for supplying the original compound on which the data were measured. We thank the Fondazione Istituto Italiano di Tecnologia (IIT) (project SEED 2009 "HELYOS"), the Ministero dell'Università e della Ricerca (MIUR) (PRIN 2008, grant number 2008CSNZFR) and the Fondazione Carisbo for financial support.

[1] J. P. Sauvage, J. P. Collin, J. C. Chabron, S. Guillerez, C. Coudret, V. Balzani, F. Barigelletti, L. De Cola, L. Flamigni, *Chem. Rev.* **1994**, *94*, 993–1019.
[2] V. Balzani, A. Juris, M. Venturi, S. Campagna, S. Serroni, *Chem. Rev.* **1996**, *96*, 759–833.
[3] P. Besler, S. Bernhard, C. Blum, A. Beyeler, L. De Cola, V. Balzani, *Coord. Chem. Rev.* **1999**, *190–192*, 159–169.
[4] a) A. Juris, V. Balzani, F. Barigelletti, S. Campagna, P. Belser, A. von Zelewsky, *Coord. Chem. Rev.* **1988**, *84*, 85–277; b) M. Maestri, N. Armaroli, V. Balzani, E. C. Constable, A. M. W. Cargill Thompson, *Inorg. Chem.* **1995**, *34*, 2759–2767; c) V. Balzani, G. Bergamini, F. Marchioni, P. Ceroni, *Coord. Chem. Rev.* **2006**, *250*, 1254–1266.
[5] S. Campagna, F. Puntoriero, F. Nastasi, G. Bergamini, V. Balzani, *Top. Curr. Chem.* **2007**, *280*, 117–214.
[6] K. Kalyanasundaram, M. Grätzel, *Coord. Chem. Rev.* **1998**, *77*, 347–414.
[7] A. Vlček Jr., S. Záliš, *Coord. Chem. Rev.* **2007**, *251*, 258–287.
[8] B. O'Regan, M. Grätzel, *Nature* **1991**, *353*, 737–740.
[9] M. Grätzel, *Nature* **2001**, *414*, 338–344.
[10] M. K. Nazeeruddin, A. Kay, I. Rodicio, R. Humphry-Baker, E. Müller, P. Liska, N. Vlachopoulos, M. Grätzel, *J. Am. Chem. Soc.* **1993**, *115*, 6382–6390.
[11] M. K. Nazeeruddin, S. M. Zakeeruddin, R. Humphry-Baker, S. I. Gorelsky, A. B. P. Lever, M. Grätzel, *Coord. Chem. Rev.* **2000**, *208*, 213–225.
[12] M. K. Nazeeruddin, F. De Angelis, S. Fantacci, A. Selloni, G. Viscardi, P. Liska, S. Ito, B. Takeru, M. Grätzel, *J. Am. Chem. Soc.* **2005**, *127*, 16835–16847.
[13] a) R. Ballardini, V. Balzani, A. Credi, M. T. Gandolfi, M. Venturi, *Acc. Chem. Res.* **2001**, *34*, 445–455; b) V. Balzani, A. Credi, M. Venturi, *Molecular Devices and Machines – Concepts and Perspectives for the Nano World*, Wiley-VCH, Weinheim, Germany, **2008**; c) M. Amelia, L. Zou, A. Credi, *Coord. Chem. Rev.* **2010**, *254*, 2267–2280; d) W. R. Browne, N. M. O'Boyle, J. J. McGarvery, G. J. Vos, *Chem. Soc. Rev.* **2005**, *34*, 641–663.
[14] a) S. Fantacci, F. De Angelis, J. Wang, S. Bernhard, A. Selloni, *J. Am. Chem. Soc.* **2004**, *126*, 9715–9723; b) N. Tuccitto, V. Ferri, M. Cavazzini, S. Quici, G. Zhavnerko, A. Licciardello, M. A. Rampi, *Nat. Mater.* **2009**, *8*, 41–46; c) O. Wenger, *Coord. Chem. Rev.* **2009**, *253*, 1439–1457.
[15] V. Balzani, S. Campagna, G. Denti, A. Juris, S. Serroni, M. Venturi, *Acc. Chem. Res.* **1998**, *31*, 26–34.
[16] V. Balzani, P. Ceroni, A. Juris, M. Venturi, S. Campagna, F. Puntoriero, S. Serroni, *Coord. Chem. Rev.* **2001**, *219–221*, 545–572.
[17] L. E. Joyce, J. D. Aguirre, A. M. Angeles-Boza, A. Chouai, P. K.-L. Fu, K. R. Dunbar, C. Turro, *Inorg. Chem.* **2010**, *49*, 5371–5376.
[18] L. H. Zhang, F. Tsow, E. Forzani, N. J. Tao, *Chem. Commun.* **2010**, *46*, 3333–3335.
[19] H. D. Batey, A. C. Whitwood, A. K. Duhme-Klair, *Inorg. Chem.* **2007**, *46*, 6516–6528.
[20] K. E. Erkkila, D. T. Odom, J. K. Barton, *Chem. Rev.* **1999**, *99*, 2777–2796.
[21] I. Haq, P. Lincoln, D. Suh, B. Norden, B. Z. Chowdhry, J. B. Chaires, *J. Am. Chem. Soc.* **1995**, *117*, 4788–4796.
[22] a) E. C. Constable, C. E. Housecroft, A. Cargill Thompson, P. Passaniti, S. Silvi, M. Maestri, A. Credi, *Inorg. Chim. Acta* **2007**, *360*, 1102–1110; b) S. Silvi, E. C. Constable, C. E. Housecroft, J. E. Beves, E. L. Dunphy, M. Tomasulo, F. M. Raymo, A. Credi, *Chem. Eur. J.* **2009**, *15*, 178.
[23] S. Fantacci, F. De Angelis, A. Selloni, *J. Am. Chem. Soc.* **2003**, *125*, 4381–4387.
[24] S. Fantacci, F. De Angelis, A. Sgamellotti, A. Marrone, N. Re, *J. Am. Chem. Soc.* **2005**, *127*, 14144–14145.
[25] S. Fantacci, F. De Angelis, A. Sgamellotti, N. Re, *Chem. Phys. Lett.* **2004**, *396*, 43–48.
[26] F. De Angelis, S. Fantacci, A. Selloni, *Chem. Phys. Lett.* **2004**, *389*, 204–208.
[27] F. De Angelis, S. Fantacci, A. Selloni, M. K. Nazeeruddin, *Chem. Phys. Lett.* **2005**, *415*, 115–120.
[28] C. Barolo, M. K. Nazeeruddin, S. Fantacci, D. Di Censo, P. Comte, P. Liska, G. Viscardi, P. Quagliotto, F. De Angelis, S. Ito, M. Grätzel, *Inorg. Chem.* **2006**, *45*, 4642–4653.
[29] M. K. Nazeeruddin, T. Bessho, L. Cevey, S. Ito, C. Klein, F. De Angelis, S. Fantacci, P. Comte, P. Liska, H. Imai, M. Grätzel, *J. Photochem. Photobiol. A: Chem.* **2007**, *185*, 331–337.
[30] F. De Angelis, S. Fantacci, A. Sgamellotti, *Theor. Chem. Acc.* **2007**, *117*, 1093–1104.
[31] M. J. Frisch, G. W. Trucks, H. B. Schlegel, G. E. Scuseria, M. A. Robb, J. R. Cheeseman, J. A. Montgomery Jr., T. Vreven, K. N. Kudin, J. C. Burant, J. M. Millam, S. S. Iyengar, J. Tomasi, V. Barone, B. Mennucci, M. Cossi, G. Scalmani, N. Rega, G. A. Petersson, H. Nakatsuji, M. Hada, M. Ehara, K. Toyota, R. Fukuda, J. Hasegawa, M. Ishida, T. Nakajima, Y. Honda, O. Kitao, H. Nakai, M. Klene, X. Li, J. E. Knox, H. P. Hratchian, J. B. Cross, V. Bakken, C. Adamo, J. Jaramillo, R. Gomperts, R. E. Stratmann, O. Yazyev, A. J. Austin, R. Cammi, C. Pomelli, J. W. Ochterski, P. Y. Ayala, K. Morokuma, G. A. Voth, P. Salvador, J. J. Dannenberg, V. G. Zakrzewski, S. Dapprich, A. D. Daniels, M. C. Strain, O. Farkas, D. K. Malick, A. D. Rabuck, K. Raghavachari, J. B. Foresman, J. V. Ortiz, Q. Cui, A. G. Baboul, S. Clifford, J. Cioslowski, B. B. Stefanov, G. Liu, A. Liashenko, P. Piskorz, I. Komaromi, R. L. Martin, D. J. Fox, T. Keith, M. A. Al-Laham, C. Y. Peng, A. Nanayakkara, M. Challacombe, P. M. W. Gill, B. Johnson, W. Chen, M. W. Wong, C. Gonzalez, J. A. Pople. *Gaussian 03*, rev C.02, Gaussian, Inc., Wallingford, CT, **2004**.
[32] A. D. Becke, *J. Chem. Phys.* **1993**, *98*, 5648–5652.
[33] P. J. Hay, W. R. Wadt, *J. Chem. Phys.* **1985**, *82*, 299–310.
[34] a) V. A. Rassolov, M. A. Ratner, J. A. Pople, P. C. Redfern, L. A. Curtiss, *J. Comput. Chem.* **2001**, *22*, 976–984; b) V. A. Rassolov, J. A. Pople, M. A. Ratner, T. L. Windus, *J. Chem. Phys.* **1998**, *109*, 1223–1229.
[35] a) S. Miertš, E. Scrocco, J. Tomasi, *Chem. Phys.* **1981**, *55*, 117–169; b) M. Cossi, V. Barone, R. Cammi, J. Tomasi, *Chem. Phys. Lett.* **1996**, *255*, 327–335.
[36] M. Cossi, V. Barone, *J. Chem. Phys.* **2001**, *115*, 4708–4717.
[37] E. C. Constable, C. E. Housecroft, M. Neuburger, S. Schaffner, F. Schaper, *Inorg. Chem. Commun.* **2006**, *9*, 616–619.
[38] D. C. Craig, M. L. Scudder, W. A. McHale, H. A. Goodwin, *Aust. J. Chem.* **1998**, *51*, 1131–1140.
[39] a) E. M. Kober, J. V. Caspar, R. S. Lumpkin, T. J. Meyer, *J. Phys. Chem.* **1986**, *90*, 3722–3734; b) B. R. Henry, W. Siebrand, in *Organic Molecular Photophysics* (Ed.: J. B. Birks), Wiley, New York, **1973**, Vol. 1, Ch. 4; c) K. F. Freed, J. Jortner, *J. Chem. Phys.* **1970**, *52*, 6272–6291; d) M. Bixon, J. Jortner, *J. Chem. Phys.* **1968**, *48*, 715–726.
[40] a) F. Santoro, R. Improta, A. Lami, J. Bloino, V. Barone, *J. Chem. Phys.* **2007**, *126*, 084509–084521; b) F. De Angelis, F. Santoro, M. K. Nazeeruddin, V. Barone, *J. Phys. Chem. B* **2008**, *112*, 13181–13183.

Received: December 2, 2010
Published Online: February 18, 2011

